ACS OMEGA

http://pubs.acs.org/journal/acsodf

Article

Cleavage of Abasic Sites in DNA by an Aminoquinoxaline Compound: Augmented Cytotoxicity and DNA Damage in Combination with an Anticancer Drug Chlorambucil in Human Colorectal Carcinoma Cells

Chandra Sova Mandi, Tridib Mahata, Dipendu Patra, Jeet Chakraborty, Achyut Bora, Ritesh Pal, and Sanjay Dutta*

Cite This: *ACS Omega* 2022, 7, 6488−6501

Read Online

ACCESS | Metrics & More | Article Recommendations | Supporting Information

ABSTRACT: The elevated level of endogenous oxidative DNA damage and spontaneous deamination of DNA bases in cancer cells substantially increase the abasic sites in DNA via base excision repairs (BERs). Thus, the predominant BER pathway is a favorable target for cancer therapy. Interestingly, elevated levels of glutathione (GSH) in certain cancer cells, such as colon cancer, are associated with acquired resistance to several chemotherapeutic agents, which increase the difficulty for the treatment of cancer. Here, we have reported an ideal nitro group-containing monoquinoxaline DNA intercalator (**1d**), which is reduced into a fluorescent quinoxaline amine (**1e**) in the presence of GSH; concurrently, **1e** (∼100 nM concentration) selectively causes the *in vitro* cleavage of abasic sites in DNA. **1e** also binds to the tetrahydrofuran analogue of the abasic site in the nanomolar to low micromolar range depending on the nucleotide sequence opposite to the abasic site and also induces a structural change in abasic DNA. Furthermore, the amine compound (**1e**) augments the response of the specific bifunctional alkylating drug chlorambucil at a much lower concentration in the human colorectal carcinoma cell (HCT-116), and their combination shows a potential strategy for targeted therapy. Alone or in combination, **1d** and **1e** lead to a cascade of cellular events such as induction of DNA double-stranded breaks and cell arrest at G_0/G_1 and G_2/M phases, eventually leading to apoptotic cell death in HCT-116 cells. Hence, the outcome of this study provides a definitive approach that will help optimize the therapeutic applications for targeting the abasic site in cancer cells.

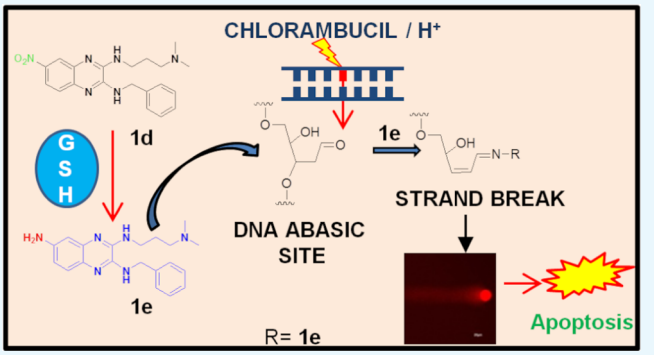

INTRODUCTION

Abasic, also known as AP (apurinic or apyrimidic), sites are the most frequent DNA lesions that are generated in living cells through various mechanisms.[1,2] These lesions are produced by loss of bases via an incision of the *N*-glycosidic bond between a base and its deoxyribose residue in DNA.[3] Endogenous DNA abasic sites are generated by the base excision repair (BER) pathway through enzymatic action, as the DNA *N*-glycosylases can recognize the damaged DNA bases and remove the abnormal bases in DNA. This repair process can lead to cleavage of the phosphodiester bond adjoining the DNA lesions via the AP endonucleases enzyme.[4] Furthermore, this process is significantly accelerated by physical (e.g., UV and γ-rays) or chemical agents (e.g., alkylating agents and carcinogens).[5−7] Consequently, it is estimated that approximately 10 000 AP sites are generated spontaneously per cell per day.[8−10]

At physiological pH, the frequency of an AP site formation is higher for purine residues (depurination) as compared to pyrimidine residues (depyrimidination). Moreover, depurination mainly occurs due to modifications at the N7 or N3 position of guanine and adenine in DNA, respectively, although guanines are released faster than adenines during the spontaneous hydrolysis process.[11] With respect to chemical structure stability, the structure of the abasic site exists in an equilibrium between the ring-opened aldehyde (1%) and the ring-closed acetal form (99%)[12] (Scheme 1). In addition, these abasic sites in DNA can lead to DNA interstrand cross-links.[13] Notably, this noninformative damage has to be repaired before a cell undergoes replication and transcription. Thus, unrepaired DNA damage owing to mutagenesis through

Received: September 8, 2021
Accepted: December 7, 2021
Published: February 18, 2022

https://doi.org/10.1021/acsomega.1c04962
ACS Omega 2022, 7, 6488−6501

Scheme 1. Equilibrium States of an Abasic (AP) Site

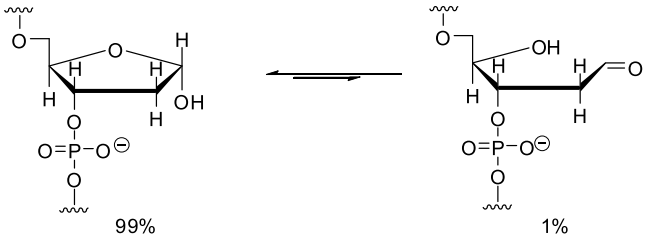

nucleotide misincorporation can eventually lead to genomic instability, and it promotes cancer development.[14,15]

Most cancer cells often exhibit specific deformities in their DNA and DNA repair pathways.[16] Nevertheless, the elevated levels of endogenous oxidative damage and the inefficiency of the DNA repair system may lead to AP site formation in cancer cells. It has been reported that cell lines derived from non-Hodgkin B-cell lymphomas or leukemias (B-NHLs) contain elevated levels of abasic sites compared to normal circulating B-cells. Such cells are thus highly selective for targeting AP sites in B-cell cancers.[17] Endogenous AP sites are known to interfere with the function of many enzymes such as topoisomerase (I/II) and BER proteins (APE1, PARP-1, DNA pol β).[18−20] Concomitantly, the BER pathway tries to repair this lesion. In contrast, upregulated BER pathways confer therapeutic resistance via abasic site formation. BER is one of the pathways that is involved in the repair of damaged DNA or lesions caused by the action of DNA-alkylating molecules and therefore can be targeted for the discovery of anticancer drugs.[21−25] Thus, inhibition of the BER pathway sensitizes the cancer cells toward the effect of DNA-alkylating agents in certain cancers. Small molecules that covalently bind with abasic sites and block the BER pathway are of great interest.

Some small compounds such as polyamines, a tripeptide (Lys-Trp-Lys), and DNA intercalators (9-aminoellipticine or 3-aminocarbazole) have been reported to cleave specifically at AP sites through the β elimination process.[26−29] Caron et al. have developed napthalenophanes that bind at the abasic sites in DNA and inhibit APE1-induced hydrolysis.[30] Additionally, another APE1 inhibitor, methoxyamine (MX), which forms a covalent bond with abasic aldehyde, impedes the DNA backbone cleavage by APE1.[31] Also, methoxyamine in combination with temozolomide showed activities both *in vitro* and in human tumor xenograft models.[32] However, 9-aminoellipticine has been shown to increase the cytotoxic activity of an alkylating agent, dimethyl sulfate, in *E. coli*.[33] Thus, designing and developing small compounds that can selectively recognize AP sites and imbalance the DNA repair processes might provide an exemplary strategy. In this aspect, Lhomme and co-workers synthesized artificial nucleases that can bind and cause cleavage of abasic sites of DNA *in vitro* at nanomolar concentrations.[34] However, not much work has been done on the cellular DNA damage or anticancer activities of these artificial nucleases. Another approach is to design small compounds that can interfere with the repair of AP sites efficiently enough to potentiate the cytotoxic effects of radiations or alkylating agents for therapeutic advancements in cancers.

We have previously shown that a nitro-containing monoquinoxaline compound (**1d**, Scheme 2) having a mandatory benzyl moiety and a dimethylamine tail is capable of intercalating dsDNA, inducing a structural change in DNA

Scheme 2. Plausible Mechanism of DNA Cleavage at the AP Site by 1e

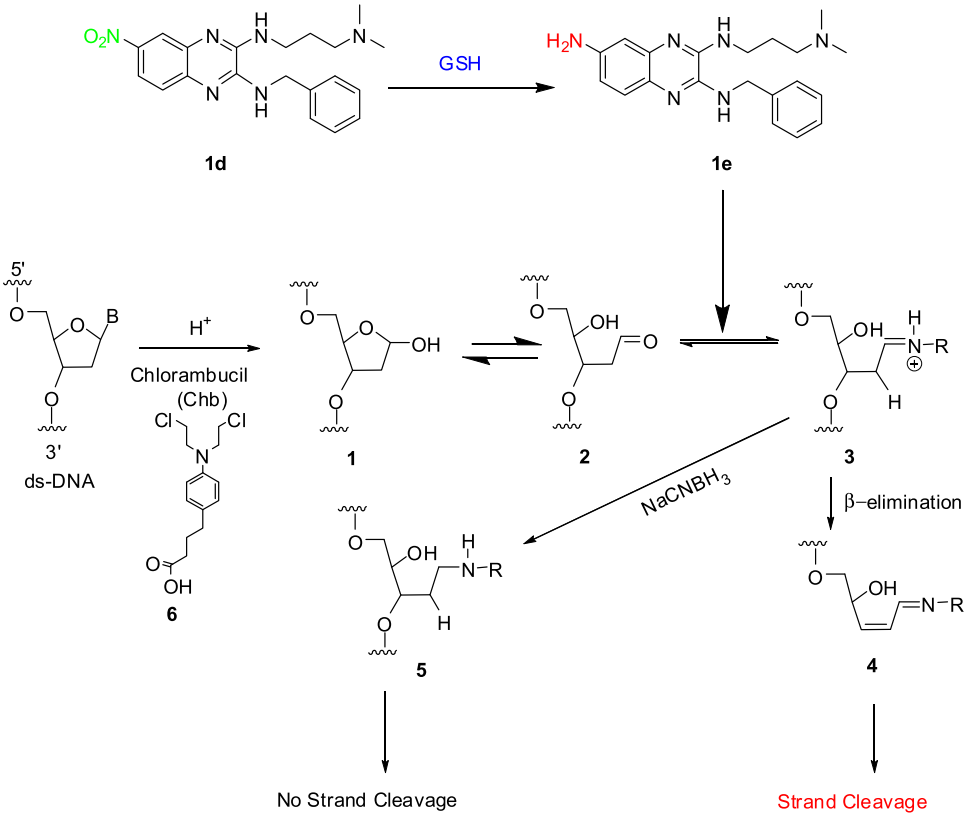

https://doi.org/10.1021/acsomega.1c04962
ACS Omega 2022, 7, 6488−6501

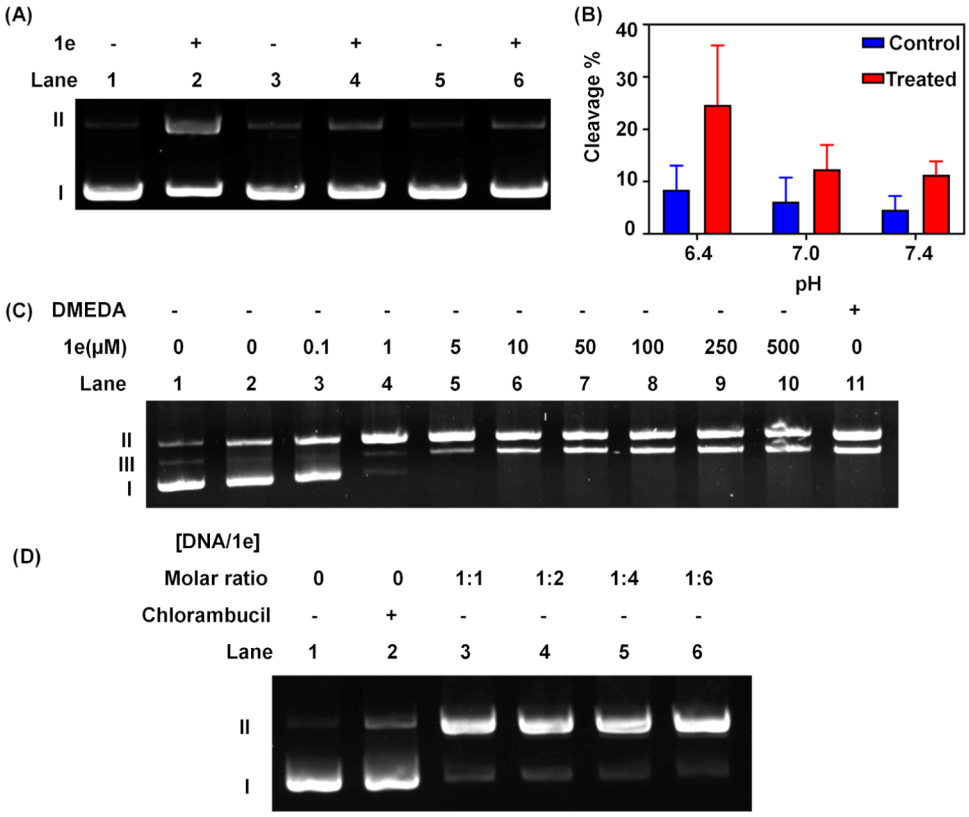

Figure 1. (A) pH-Dependent pBR322 plasmid DNA (1 μg) cleavage in the presence of **1e**. Lanes 1, 3, and 5 with control (no treatment). Lanes 2, 4, and 6 with **1e** (500 μM) at pH 6.4, pH 7.0, and pH 7.4, respectively. Reactions were performed in 50 mM sodium phosphate buffer containing 1% DMSO, incubated at 37 °C for 16 h and analyzed by agarose gel electrophoresis. (B) Representative graph of % cleavage of form II at different pH values. (C) Concentration-dependent cleavage of depurinated pBR322 plasmid at pH 7. Lane 1, native pBR322 plasmid (0.2 μg). Lane 2, control AP-plasmid (0.2 μg). Lanes 3−10, **1e** (0.1−500 μM). Lane 11, 100 mM DMEDA. Supercoiled AP-pBR322 plasmid DNA (0.2 μg) containing an average of 1.8 apurinic sites per DNA was incubated with various concentrations of **1e** in 50 mM sodium phosphate buffer containing 1% DMSO, incubated for 20 min at 37 °C followed by agarose gel electrophoresis analysis. (D) Effect of **1e** on chlorambucil-induced abasic sites in the pBR322 plasmid. Lane 1, control. Lane 2, with 100 μM chlorambucil. Lanes 3−6, cotreatment with chlorambucil and **1e** in 1:1, 1:2, 1:4, 1:6 (DNA bp)/**1e** ratios. Reactions were performed in 50 mM sodium phosphate buffer (pH 7) containing 1% DMSO, incubated at 37 °C for 16 h and analyzed by agarose gel electrophoresis.

and forming a DNA superstructure at GC-rich regions. This binding event leads to histone eviction from *in vitro* assembled nucleosomes similar to the anticancer drug Doxorubicin.[35,36] Moreover, the derivatives of **1d** (nitroquinoxaline) were also able to kill certain Gram-positive and Gram-negative bacterial cells causing bacterial DNA damage and morphological alteration of bacterial cells.[37] Besides, quinoxaline derivatives of **1d** also bind to HCV RNA at the internal ribosome entry site and inhibit HCV-mediated translation and replication.[38] Subsequently, we were interested in a quinoxaline-based amine (**1e**, Scheme 2) that can selectively bind and cleave abasic sites in DNA.

In the present work, we have investigated the DNA cleaving property of **1e** (aminoquinoxaline), which can selectively bind and cleave DNA abasic sites. A schematic representation of the mechanism of DNA cleavage at the abasic site is shown in Scheme 2. Herein, we report the mechanism of **1e** to induce cleavage at depurinated plasmid DNA, ^{32}P radiolabeled abasic oligonucleotide, and alkylating agent-treated plasmid DNA. **1e** also demonstrates the increased binding for AP-DNA compared to the binding for native DNA. The base selectivity opposite to the abasic site was also studied with the oligonucleotide containing the tetrahydrofuran (THF) moiety. **1e** induces structural change in depurinated DNA compared to native plasmid DNA. We also report the reduction of the nitro-containing DNA intercalator **1d** to the corresponding amine **1e** *in vitro* in the presence of the cellular tripeptide thiol, glutathione (GSH). Reduced GSH is the most abundant cellular thiol, which is also significantly higher in different colon cancer cells such as HCT-116, as compared with normal colon cells.[39,40] As previously shown, nitro compounds are known to undergo reduction by cellular enzymes such as xanthine oxidase to the corresponding amines.[41] Thus, a higher glutathione level in HCT-116 (human colorectal cancer) cells had been exploited to explore cellular activities of the nitro compound; the reduced **1d** is the active species involved in targeting abasic sites in cellular DNA. The study also aimed to quantify the cytotoxicity and cellular DNA damage induced by **1d** and **1e**, used alone and in combination with the known anticancer drug chlorambucil *ex vivo*. Chlorambucil (**6**, Scheme 2) is an alkylating agent that belongs to the nitrogen mustard family and used in the treatment of various types of cancers.[42] Chlorambucil's activity, just like other bifunctional alkylating agents, is mediated through alkylation at the N7 position of guanine residues, which leads to DNA interstrand cross-links, and is the reasonable cause for its antitumor activities.[43−45] Chlorambucil also generates abasic sites in DNA and facilitates better DNA damage.[46,47] Although chlorambucil is regarded as

https://doi.org/10.1021/acsomega.1c04962
ACS Omega 2022, 7, 6488−6501

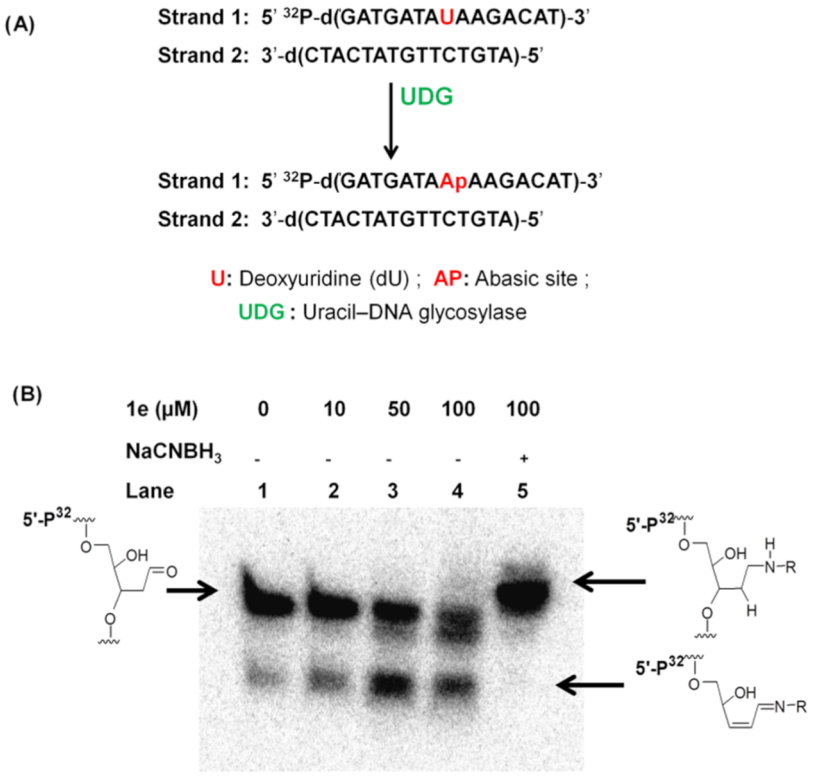

Figure 2. (A) 2′-Deoxyuridine-containing deoxyoligonucleotide duplex as a substrate. (B) The 5′-end ^{32}P-labeled AP site containing oligonucleotide was run on a 20% polyacrylamide gel containing 8 M urea after no treatment (lane 1), after treatment with 10, 50, and 100 μM with **1e** (lanes 2, 3, and 4), and after treatment with 100 μM with **1e** and 270 mM $NaCNBH_3$ (lane 5) at 37 °C.

a highly therapeutic drug, acquired resistance in cancer cells is a major concern for therapeutic purposes.[48,49] Our purpose was to effectively use a lesser concentration of chlorambucil for cellular studies to minimize the toxicity and create abasic sites, whose half-life can be reduced due to the interaction with the neighboring histone lysines in nucleosome particles in cells.[50] Overall, we report the potent anticancer activities of **1d** and **1e** and in combination with chlorambucil. The cellular activities of **1d** and **1e** investigated in HCT-116 cells show that in combination with chlorambucil, both induced massive DNA damage, leading to a cascade of cellular events and fostering cell death. This study provides a mechanism of utilization of cellular thiol for effectively targeting colon cancer cells and the usability of the combination treatment with a known anticancer drug.

RESULTS AND DISCUSSION

Cleavage at the Abasic Site Containing the pBR322 Plasmid DNA by 1e. For our study, we have synthesized the amine compound **1e** from the previously reported nitro compound **1d**.[51] Synthesis of compound **1e** is shown in Scheme S1. The nitro compound (**1d**) was converted into the corresponding amine compound (**1e**) by dissolving it in ethanol and treating it with 10% palladium activated on charcoal under a hydrogen atmosphere (yield ∼ 90%) (synthesis details in the Supporting Information).

Initially, we utilized a plasmid-based assay to investigate DNA strand cleavage by **1e**. To test the hypothesis that **1e** cleaves depurinated DNA, supercoiled pBR322 plasmid DNA (1 μg) was incubated with **1e** (500 μM) at different pH conditions at 37 °C for 16 h in 5% (v/v) DMSO. As shown in Figure 1A, more cleavage in plasmid DNA at pH 6.4 (lane 2) was observed compared to that at pH 7 (lane 4) or 7.4 (lane 6). The circular covalently closed form of the plasmid DNA (form I) is converted into the open circular form (form II) due to single-strand breaks initiated by DNA cleavage at the abasic site by **1e**. The effect of **1e** was more prevalent at pH 6.4 due to depurination occurring at lower pH forming AP sites. At lower pH, protonation causes more depurination due to protonation at the N7-guanine and N3 adenine residues in DNA, which leads further to the closed sugar ring hemiacetal and the open aldehyde forms (Scheme 1), creating an AP site. This observation shows that **1e** is capable of DNA strand cleavage at the AP site. The cleavage percentage (%) of the open circular form (form II) was calculated at different pH values (Figure 1B).

The initial observation suggests that **1e** could cleave at the AP site. To determine the effect of **1e** at the AP site, depurinated pBR322 plasmid DNA was prepared. Depurination was done under conditions of 25 mM sodium acetate, pH 4.8, 70 °C, for 20 min to generate an average of 1.8 AP sites per DNA compound as previously reported. The DNA cleavage activity was measured by incubating depurinated pBR322 plasmid DNA in the presence of varying concentrations of **1e** at 37 °C, pH 7, for 20 min. The conversion of circular covalently closed (form I) into open circular (form II) and linear (form III) forms was used to calculate relative cleavage efficiencies. In Figure 1C, the closed circular form (form I) with increasing concentrations of **1e** disappears rapidly. At 100 nM concentration (lane 3, Figure 1C), single-strand breaks become notable, and at higher concentrations (≥1 μM, lanes 4−10, Figure 1C), double-stranded breaks were significantly visible in depurinated plasmid DNA. In addition, 100 mM 1,2-dimethylethylenediamine (DMEDA, lane 11,

https://doi.org/10.1021/acsomega.1c04962
ACS Omega 2022, 7, 6488−6501

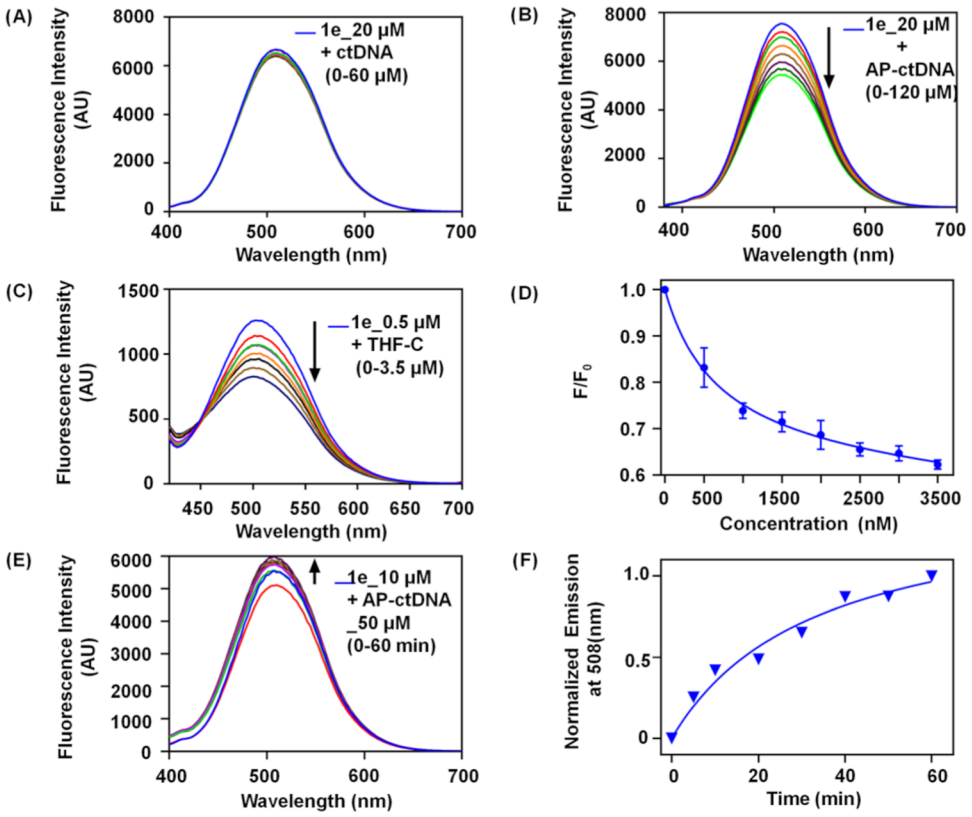

Figure 3. Fluorescence emission spectra of **1e** (20 μM) at 508 nm in the presence of various concentrations of (A) calf thymus DNA and ctDNA (0−60 μM bp), and (B) AP site containing calf thymus DNA and AP-ctDNA (0−120 μM bp). (C) Fluorescence emission spectra of **1e** (0.5 μM) upon addition of the DNA duplex with the target cytosine base opposite the AP site (0.5−3.5 μM; 5′-GATGATA**X**AAGACAT-3′/5′-ATGTCTTCTATCATC-3′, **X** = dSpacer/THF). (D) Fluorescence titration curve for **1e** (0.5 μM) with the cytosine base opposite the AP site containing the DNA duplex. F/F_0 denotes normalized fluorescence of **1e** with or without the AP-DNA duplex. Data represent the mean ± standard deviation (SD) of three individual experiments. The data were fitted via nonlinear regression based on a one-site binding model. (E) Time-dependent fluorescence emission spectra of **1e** (10 μM) upon addition of AP-ctDNA (50 μM bp). (F) Normalized fluorescence time course of **1e** binding to AP-ctDNA. The data were fitted via a nonlinear regression based on the kinetics binding equation; dissociation—one-phase exponential decay (GraphPad Prism). Measurements were done in 10 mM sodium phosphate buffer, pH 7.0 containing 10 mM NaCl and 1% DMSO at 25 °C. **1e**, λ_{ex}: 362 nm.

Figure 1C) treatment was used as a standard showing three forms of the supercoiled plasmid. Like DMEDA, **1e** (at a much lower concentration) could catalyze the β-elimination reaction (Scheme 2), leading to a DNA strand cleavage. Thus, from the result, it is evident that the **1e** compound causes a single- and double-stranded break at the AP site in the DNA strand. The cleavage activity was also studied with spermine, which showed that there was no such significant cleavage of AP sites at comparable concentrations (Figure S3A).

Alkylating agents display their toxicities through covalently binding to DNA and resulting in the loss of a base, creating an AP site.[47,48] Here, chlorambucil (**6**, Scheme 2) was used to generate abasic sites in DNA through the alkylation of N7-guanine residues in plasmid DNA. Supercoiled plasmid DNA (pBR322, 1 μg) was incubated with chlorambucil (100 μM) for 3 h at 37 °C and then was subsequently treated with varying concentrations of **1e** for 16 h. As determined by agarose gel electrophoresis, there was no significant change after only chlorambucil treatment (Figure 1D, lane 2). However, with different **1e** concentrations (Figure 1D, lanes 3−6), the cleavage band of form II increased. Figure S3B shows the varying concentrations of **1e** used as a reference to test the outcome without chlorambucil treatment. Again, there was no significant change in a single treatment with varying concentrations of **1e** (Figure S3B, lanes 2−5). Chlorambucil induces the AP site through DNA alkylation and depurination, followed by DNA strand cleavage by **1e**. Thus, both **1e** and chlorambucil in combination could be lethal to cellular purposes.

Cleavage at the AP Site of DNA via Schiff Base Formation. To test the mechanism by which **1e** forms a Schiff base intermediate, we generated an oligonucleotide duplex containing an authentic AP site by treatment of the 2′-deoxyuridine-containing oligonucleotide duplex with uracil-DNA glycosylase (UDG) (Figure 2A). Before annealing of the oligomer duplex and treatment with UDG, the single-stranded uracil-containing oligomer was 5′-end ^{32}P-labeled using a previously reported procedure. Subsequently, the 5′-end-labeled oligonucleotide was annealed with the corresponding complementary deoxyoligonucleotide containing a guanine residue opposite the uracil. Upon digestion with UDG, the ^{32}P-labeled annealed oligomer duplex contained a single AP site. In Figure 2B, the reaction of the AP-site oligomer duplex with increasing concentrations of **1e** produced a substantial amount of cleaved strand (lanes 2, 3, and 4) compared to the control reaction without **1e**-treated cells (lane 1). However, in the presence of a reducing agent sodium cyanoborohydride ($NaCNBH_3$), **1e** displayed no cleavage and there was a slight

https://doi.org/10.1021/acsomega.1c04962
ACS Omega 2022, 7, 6488−6501

decrease in the mobility of the complex formed (lane 5). These data suggest that the exocyclic amine of **1e** reacts with the aldehyde of the AP site by forming a Schiff base or an imminium-ion intermediate, which is reduced via trapping the complex with $NaCNBH_3$ (Scheme 2). Hence, the probable mechanism of strand cleavage by **1e** occurs via proton abstraction from the α-carbon of the imminium moiety, subsequently causing β-elimination of phosphate groups, which was earlier shown by agarose gel data of the AP site-containing plasmid DNA reaction with **1e**.

1e Can Discriminate between Native and AP Site-Containing DNA. To determine the binding mode of **1e**, UV−vis and fluorescence spectroscopy studies were performed. **1e** (20 μM) was titrated with increasing concentrations (0−50 μM bp) of ctDNA in sodium phosphate buffer. The absorbance maxima of **1e** at 362 nm showed no significant change with increasing concentrations of ctDNA (Figure S4A). Similarly, in fluorescence spectroscopy, **1e** (20 μM) titrated with increasing concentrations (0−60 μM bp) of ctDNA also resulted in no significant changes in the emission spectra of **1e** (Figure 3A). These results indicate that **1e** does not interact significantly with native double-stranded DNA.

Next, similar studies were performed with AP site-containing ctDNA (AP-ctDNA). The UV−vis absorbance of **1e** (20 μM) with increasing concentrations of AP-ctDNA (0−60 μM bp) displayed that there was a decrease in absorbance at 362 nm in the presence of AP-ctDNA (Figure S4B). This result indicates the interaction of compound **1e** with the AP site. The binding affinity of **1e** was determined by fluorescence spectroscopy.

The emission spectra (λ_{em} = 508 nm) of **1e** (20 μM) gradually decreased upon addition of an increasing concentration of AP-ctDNA (0−120 μM bp) (Figure 3B). This significant quenching of **1e** fluorescence intensity upon the addition of AP-ctDNA indicated an interaction between the AP-ctDNA and **1e**. In another set of fluorescence experiments, base selective binding of **1e** was studied with oligonucleotides containing tetrahydrofuran (THF) with different opposing nucleobases. THF is a structural analogue of an AP site that cannot undergo the β-elimination reaction and thus inhibits ligand-amine-mediated DNA cleavage.[52] A distinct nucleobase was incorporated opposite to the AP site-containing oligonucleotide. Figure 3C depicts the fluorescence spectra of **1e** (0.5 μM) with an increasing concentration of THF-C. Figure 3D shows the dose−response curve for **1e** (0.5 μM) with the AP site-containing DNA duplex (THF-C) having a cytosine base opposite the AP site. The data was fitted via nonlinear regression based on the one-site binding model, and the dissociation constant (K_d) values are given in Table 1. Fluorescence quenching of **1e** with the three distinct oligonucleotides where different nucleobases (G, A, and T) were placed opposite to the AP site is shown in Figure S5. The specific binding depends on the base opposite the AP site, and the best quenching is seen with the cytosine base followed by thymine, adenine, and guanine. Thus, the binding of **1e** is base-specific, i.e., it depends on the target nucleobase opposite the AP site. Figure 3E shows a time-dependent increase of fluorescence due to the interaction of **1e** (10 μM) with a fixed amount of AP-ctDNA (50 μM bp), indicating the Schiff base formation that leads to DNA strand cleavage. There was no change in the emission spectrum of **1e** after the Schiff base formation. Similarly, no shift in the emission spectrum and enhancement of fluorescence was also observed when **1e** was treated with a benzaldehyde, indicating a Schiff base formation (Figure S6). Figure 3F is the normalized fluorescence time course of **1e** binding to AP-ctDNA.

1e Shows Specific Affinity for an AP Site in DNA Inducing DNA Structural Change. Circular dichroism (CD) was used to investigate the structural change of the duplex DNA upon **1e** interaction. The CD spectra of the native ctDNA titrated with different concentrations of **1e** are shown in Figure 4A. The CD spectrum of the native ctDNA is composed of a positive signal at 272 nm (base stacking) and a negative signal at 245 nm (helicity). These two CD signals are

Table 1. Dissociation Constant (K_d, μM) for 1e with AP Site-Containing Oligonucleotides Having Different Opposing DNA Bases[a]

target base	C	A	T	G
K_d	0.86 ± 0.55	1.01 ± 0.8	1.65 ± 0.49	1.79 ± 1.08

[a]K_d values were measured in sodium phosphate buffer (10 mM) containing NaCl (10 mM) and DMSO (1%) at 25 °C. The table represents the mean and the standard deviation (mean ± SD) values obtained from three individual experiments.

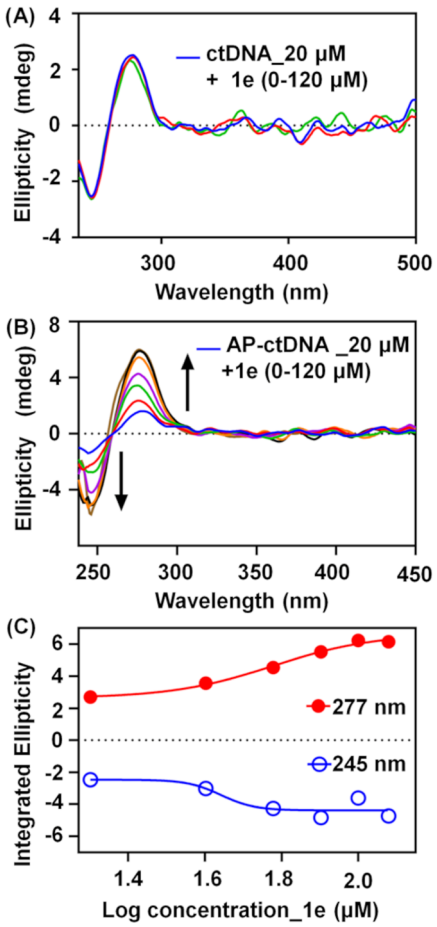

Figure 4. Circular dichroic spectral profile of (A) native ctDNA (20 μM bp) in the presence of varying concentrations of **1e** (0−120 μM). (B) AP-ctDNA (20 μM bp) in the presence of varying concentrations of **1e** (0−120 μM). (C) Integrated ellipticity of 245 and 277 nm bands of **1e** in the presence of AP-ctDNA. The experiment was performed in sodium phosphate buffer (10 mM, pH 7.0) containing 10 mM NaCl and 1% DMSO at 25 °C.

https://doi.org/10.1021/acsomega.1c04962
ACS Omega 2022, 7, 6488−6501

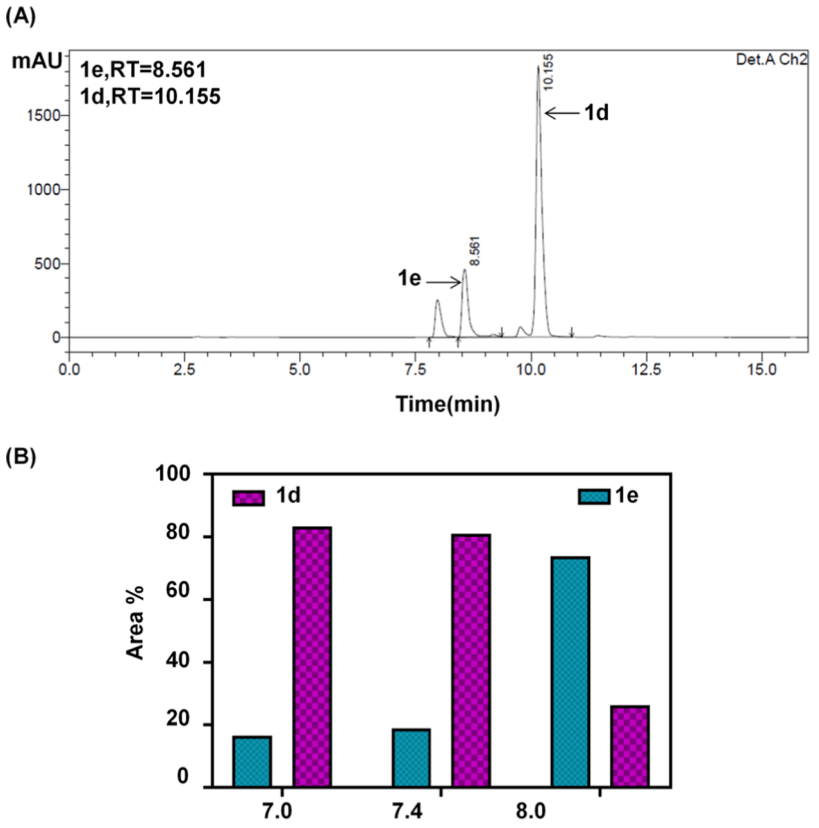

Figure 5. Representative HPLC chromatogram of (A) GSH and **1d** reaction. (B) Area % of **1d** and **1e** compounds at different pH values. The reaction of **1d** and GSH in a 1:100 ratio was performed in 50 mM sodium phosphate buffer at 37 °C, incubated for 16 h, and analyzed by a C18 reversed-phase HPLC column, detected at 254 nm. The intensity of absorbance in milli-absorbance units (mAU) was plotted against the retention time in minutes. Area % represents the percentage of area under the elution peak.

characteristic of the double-helical DNA in the B-form. Titration of increasing concentrations of **1e** with native ctDNA showed no major change in the intensity as well as a shift in the CD signal, hence indicating that **1e** does not interact with native ctDNA or alters its B-DNA conformation. Furthermore, we tested varying concentrations of the compound with AP site-containing ctDNA (AP-ctDNA). In Figure 4B, upon the addition of **1e** on AP-ctDNA, the band at 272 nm shows an increase in positive ellipticity and at 245 nm an increase in negative ellipticity with spectral shifting. Both the negative and positive bands were altered significantly by **1e**. As shown in Figure 4C, the change in the CD intensities at 272 and 245 nm showed a sigmoidal growth. This is a general indicator of a complex formation between the AP-ctDNA and the compound **1e**, showing the possible stacking of **1e** within DNA base pairs due to intercalation. Also, there is a change in the helicity of the B-form DNA. Overall from the data, it is understood that the binding affinity of the **1e** compound with AP site-containing DNA is stronger than the native DNA, as seen earlier from the fluorescence data.

Formation of 1e from the Reaction between Biological Thiol Glutathione (GSH) and 1d. The reaction of a nitroquinoxaline derivative (**1d**) with glutathione (GSH) at physiological pH resulted in the formation of a quinoxaline amine (**1e**); this hypothesis was analyzed using reverse-phase HPLC to monitor the compound generation. The HPLC chromatogram as shown in Figure 5A was obtained via incubating **1d** with GSH (1:100) in a sodium phosphate buffer (pH 7, 50 mM) for 16 h at 37 °C. The reaction mixture resulted in two major products, which eluted at 8.5 and 10.1 min, identified as **1e** and **1d**, respectively. Alternately, both **1e** and **1d** compounds were synthesized, used as standards, and analyzed in the same HPLC method without GSH (Figure S7A,B). The similarity in the retention time showed that the product at 8.5 min is **1e** and the one at 10.1 min is **1d**. The corresponding fractions were collected and analyzed by ESI-MS for further confirmation.

Further, a pH-dependent analysis was performed for **1d** and GSH reactions. The reaction was monitored at three different pH values (7, 7.4, 8) in sodium phosphate buffer at 37 °C for 16 h. Based on the results, an area % vs pH was plotted (Figure 5B). At pH 8, the yield of **1e** was found to be significantly higher than at pH 7 or 7.4.

In a separate experiment, the DNA cleavage/intercalation was investigated with **1d** (with and without GSH) and **1e** with supercoiled pBR322 plasmid DNA (1 μg) at pH 6.4, 37 °C for 16 h. The reaction was monitored by agarose gel electrophoresis, and the results were analyzed after ethidium bromide staining. **1d** is a reported DNA intercalator[35] but was unable to cleave supercoiled plasmid DNA at pH 6.4 (lane 2, Figure S8). In the presence of GSH, **1d** causes a prominent DNA cleavage (lane 3, Figure S8), and this is similar to the synthesized **1e**-treated plasmid (lane 4, Figure S8). Both of them cause an increase in cleaved DNA (form II) over supercoiled DNA (form I). The results of the **1d** and GSH reaction cleaving the plasmid DNA support the observation of *in situ* formation of **1e** as shown through HPLC experiments.

https://doi.org/10.1021/acsomega.1c04962
ACS Omega 2022, 7, 6488−6501

Cytotoxicity of 1d Is Higher in Colon Cancer Cells with Elevated GSH Levels. We first investigated the antiproliferative activities of **1d** and **1e** and in combination with chlorambucil (**chb**) against different cancer cell lines. As mentioned earlier, different types of cancer cells have varying concentrations of GSH levels. To verify our hypothesis regarding the GSH-dependent cytotoxicity on cancer cells, we investigated the cellular viability of different cells (human colorectal carcinoma (HCT-116), human small lung carcinoma (A549), and human embryonic kidney (HEK 293) cells). The cellular viability was measured using the colorimetric MTT assay, after incubating the cells with different concentrations of **1d** and **1e** for 24 h. Meanwhile, in the combination treatment, cells were treated with chlorambucil to test whether this therapeutic drug could potentiate the cytotoxicity of **1d** and **1e**. For the combination treatment, cells were pretreated with chlorambucil (200 μM) for 2 h and then replaced with fresh media. Subsequently, different concentrations of **1d** and **1e** were added separately in separate experiments. For only chlorambucil treatment, different concentrations of **chb** were added and incubated for 24 h. As shown in Table 2, the IC_{50} values were observed at 2.2 and 32 μM in **1d** and **1e**, respectively, in HCT-116 cell lines. **1d** exhibited a higher antiproliferative activity against HCT-116 compared to A549 and HEK 293 cells. However, **1e** demonstrated a lesser antiproliferative activity in these cells as compared to **1d**. The higher cytotoxicity of **1d** is presumably due to the DNA intercalative[35] and structural change property of **1d** as compared to **1e**. **1d** causes a structural change in native ctDNA[35] and also abasic DNA (Figure S9), whereas **1e** causes no structural change in DNA or DNA intercalation with normal ctDNA but enhances the base stacking of abasic DNA (Figure 4). DNA intercalation by **1d** induces more double-stranded breaks and cytotoxicity as compared to **1e**. Also, **1d** is more hydrophobic than **1e**, which is a diamine, and the cellular penetration properties of both of the compounds might be different. However, **1e** has better activity in HCT-116 compared to A549 and HEK 293 cell lines. These observations suggest that both compounds possess a strong cytotoxicity and were somewhat more selective against HCT-116 cells. In Table 3, the IC_{50} values observed in the combination treatments were 0.83 and 4.7 μM in **1d** and **1e**, respectively, with chlorambucil against HCT-116 cell lines. While **Chb**-alone treatment with different concentrations for 24 h showed a weaker antiproliferative activity in HCT-116 cell lines (Table 3), **1d** with **chb** exhibited a more potent antiproliferative activity than **1e** with **chb**. The cytotoxicity effects of combination treatments are significantly higher than the individual treatments of **1d** and **1e**, indicating enhanced potencies of **1d** and **1e** in the presence of DNA-alkylating agents.

Table 2. IC_{50} Values of 1d and 1e in Human Colorectal Carcinoma (HCT-116), Human Small Lung Carcinoma (A549), and Human Embryonic Kidney (HEK 293) Cells[a]

	IC_{50} (μM) of compounds	
cell line	1d	1e
HCT-116	2.2 ± 2	32 ± 2
A549	8.9 ± 1.9	46 ± 1.8
HEK 293	11.7 ± 1.9	>50

[a]Cells were incubated with indicated compounds at different concentrations for 24 h, and cell viability was determined by the MTT assay. Data were expressed as the mean ± SD of each group of cells from three individual experiments.

Table 3. IC_{50} Values of 1d and 1e in Combination with Chlorambucil in Human Colorectal Carcinoma (HCT-116)[a]

	IC_{50} (μM) of compounds		
cell line	chlorambucil (Chb)	1d-Chb[a]	1e-Chb[a]
HCT-116	440 ± 1.8	0.83 ± 2.2	4.69 ± 3.5

[a]Cells were pretreated with chlorambucil (200 μM) for 2 h and subsequently with indicated compounds separately for 24 h. Data is expressed in mean ± SD.

1d and 1e and Also in Combination with Chlorambucil Induce DNA Damage and Cell-Cycle Arrest. We assessed the DNA damage by compounds **1d** and **1e** in HCT-116 cells through γ-H2AX immunofluorescence microscopy. The formation of γ-H2AX specific foci in cell nuclei is one of the characteristic morphological features of DNA damage. During the exposure of mammalian cells to compounds that cause DNA double-stranded breaks (DSBs), the variant histone H2AX is phosphorylated and, subsequently, γ-H2AX foci are formed.[53,54] It has been reported that DSBs can occur as a result of abasic site formation through the DNA damage repair pathway.[55] As shown in Figure 6A, the treatment of the compounds activated DNA damage in the nucleus of HCT-116 cells. The cells were treated at IC_{50} concentrations of **1d** and **1e** alone for 12 h. For combination treatment, after the initial chlorambucil (200 μM) treatment for 2 h, followed by removing the media, **1d** and **1e** were added separately at IC_{50} concentrations and incubated for 12 h. For comparison with combination treatment only chlorambucil-treated cells (200 μM for 2 h) were used. The γ-H2AX foci were noticeable after **1d** and **1e** treatment separately but were primarily absent in the untreated control cells. It has been reported that DSBs can occur as a result of abasic sites and DNA interstrand cross-link formation during its repair. The treatment of cells with chlorambucil at 200 μM for 2 h resulted in no significant γ-H2AX foci. In contrast, the combination treatment enhanced the γ-H2AX foci in the cells compared to the monotreatment, leading to more cytotoxic DNA damage. The quantification of γ-H2AX is shown in Figure S10.

To further elucidate the impact of the compounds on DNA damage in HCT-116 cells, we performed an alkaline comet assay. The formation of the tail in the alkaline comet assay depicts both single- and double-stranded DNA breakage, producing short DNA fragments. Cells were treated at IC_{50} concentrations of **1d** and **1e** and with chlorambucil (200 μM) for the combination treatment and analyzed by the comet assay after 12 h of treatment. As shown in Figure 6B, in the untreated control cells, no DNA damage was detected and the DNA remained intact. At the respective IC_{50} concentrations of compounds **1d** and **1e**, DNA-stranded breaks resulted in truncated DNA fragments that were visible as distinct comet tails. **1d** displayed less damage and less DNA migration as compared to **1e**, and chlorambucil showed no such DNA damage and migration. However, combination of chlorambucil with **1d** produced efficient DNA damage, and a similar outcome was obtained in combination with **1e**. The combined treatments of **1e** with chlorambucil yielded a longer comet tail in HCT-116, thus asserting the enhanced DNA damage by combination treatment in the cells.

https://doi.org/10.1021/acsomega.1c04962
ACS Omega 2022, 7, 6488−6501

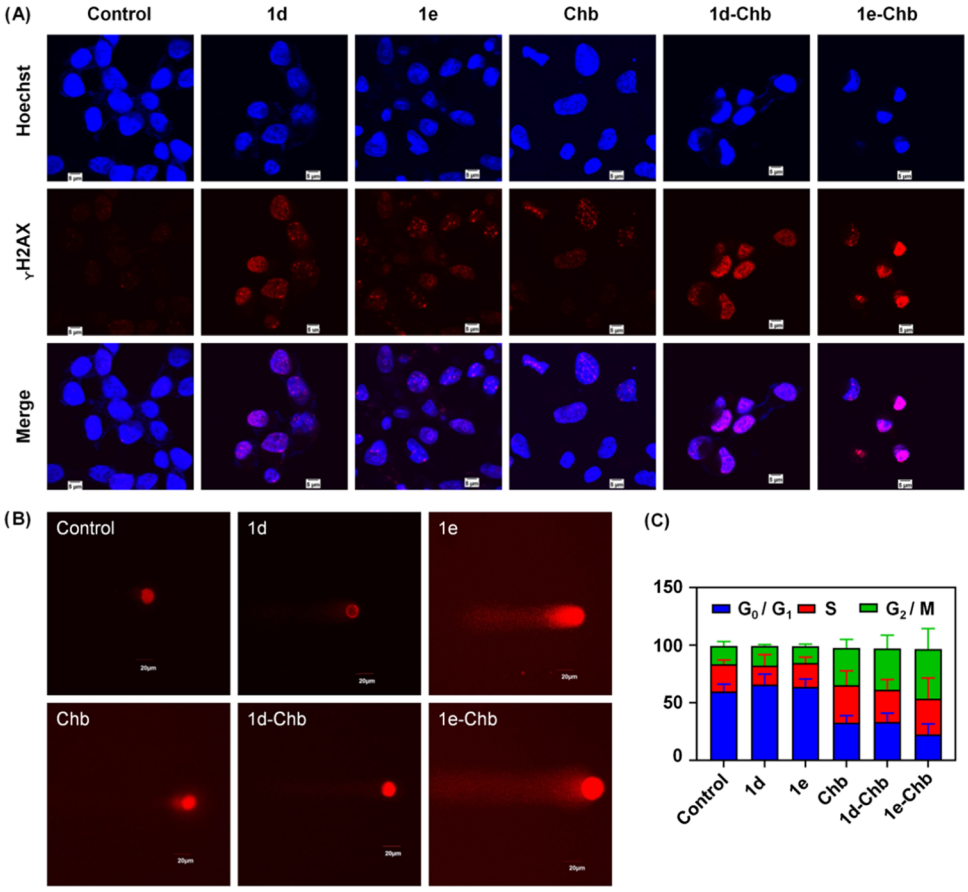

Figure 6. Representative images of (A) γ-H2AX foci (red) in HCT-116 cells after indicated treatment. Hoechst (blue) was used to stain the nucleus. Scale bar is 5 μm. Cells were treated with **1d** and **1e** alone for 12 h. For combination treatment, chlorambucil was added at 200 μM for 2 h, followed by the addition of IC_{50} concentration of **1d** and **1e**. (B) Alkaline comet assay performed in HCT-116 cells. Scale bar is 20 μm. (C) Cell-cycle analysis by a flow cytometer. Each bar represents the mean ± SD of the data obtained from three independent experiments.

To investigate whether **1e** can induce cell-cycle arrest of HCT-116 cells, which contributes to growth inhibition, flow cytometry analysis was performed. The cells were treated with IC_{50} concentrations of **1d** and **1e** compounds for 12 h. For combination, cells were treated with 200 μM chlorambucil for 2 h before the addition of **1d** and **1e** at IC_{50} concentration for 12 h. Flow cytometric analysis of the cells stained with propidium iodide (PI) was performed. In Figure 6C, the percentage of cells with **1d**-treated cells shows that the accumulation of cells at the G_0/G_1 phase increases to 56.4% compared to untreated control cells (52.6%). Similarly, the percentage of cells with **1e**-treated cells increased to 57.3% at the G_0/G_1 phase. However, chlorambucil treatment showed an increased accumulation of cells in the S phase (43.7%) compared to untreated control cells (27.2%). When treated with **1d** and chlorambucil together, the cells accumulated more at the G_2/M phase (27.4%) compared to untreated control cells (19.8%). Interestingly, a much higher G_2/M arrest was observed with **1e** and chlorambucil treatment, where cells accumulating at the G_2/M phase increased to 62.7%. The combination treatment induced cell-cycle arrest in HCT-116 cells in the G_2/M phase, whereas single compound treatment induced it at the G_0/G_1 phase. These results suggest that combination treatment inhibits cell-cycle progression associated with mitotic division interference. This indicates that the generation and cleavage of abasic sites after chlorambucil treatment by **1d** and **1e** generated more damaged and unrepaired DNA and had an impact on the cell cycle during mitotic division. However, single compound treatments induced arrest of cell-cycle progression, hampering the prior preparation of DNA synthesis in the S phase.

1d and 1e and Also in Combination with Chlorambucil Promote Apoptosis. Extended cell-cycle arrest can lead to cell death, and the resulting consequences primarily due to apoptosis induced by the compounds were investigated. Apoptosis is the process of programmed cell death. Apoptotic cells were recognized by the translocation of a phospholipid, phosphatidylserine (PS), from the inner face of the plasma member to the outer cell surface. A protein, Annexin-V conjugated FITC, binds to PS, and the cells stained with propidium iodide (PI) were analyzed through flow cytometry. As only the damaged cell membrane can take up PI, this can help in distinguishing among early apoptotic, late apoptotic, and necrotic cells. HCT-116 cells were treated with different compounds for 16 h. As depicted in Figure 7, the treatment slightly increased the early apoptotic cell population in **1d** (11.7%), **1e** (13.2%), **1d**-chlorambucil (14.3%), **1e**-chlorambucil (22.4%), and lesser chlorambucil (9.5%), compared to the untreated control (1.5%). Furthermore, the late apoptotic cell population was observed in **1d** (1%), chlorambucil (2.1%), and **1d**-chlorambucil (3.8%) and with a huge increase in **1e** (29.6%) as well as in **1e**-chlorambucil (51.8%), in comparison to the untreated control (0.6%) cells. These results suggest that

https://doi.org/10.1021/acsomega.1c04962
ACS Omega 2022, 7, 6488−6501

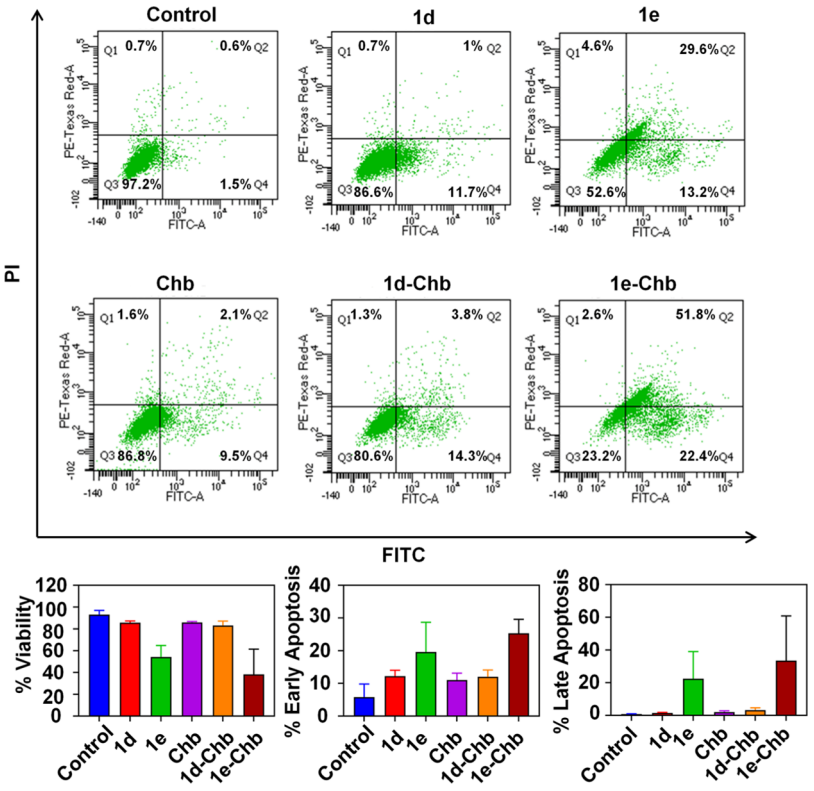

Figure 7. Flow cytometry analysis of Annexin-V and PI stained on HCT-116 cells. The four quadrants of each histogram depict viable cells (Q3, lower left quadrant), early apoptotic cells (Q4, lower right quadrant), late apoptotic cells (Q2, upper right quadrant), and necrotic cells (Q1, upper left quadrant). The percentage of apoptotic cells by the treatment of various compounds in the cells is shown below. The data represent the mean ± SD value.

HCT-116 cells undergo apoptosis when treated alone and in combination with chlorambucil.

Further, evidence against apoptosis that occurred during the treatment of HCT-116 cells was confirmed by the TUNEL assay (Figure S11). The TUNEL assay is an indicator of apoptosis accompanied by DNA fragmentation. The TUNEL assay utilizes the free 3′-OH end of the nicked DNA to insert fluorescent nucleotides catalyzed by the terminal deoxynucleotidyl transferase (TdT). The assay was performed in HCT-116 cells with IC_{50} concentrations of **1d** and **1e** for 12 h. For combination treatment, cells were treated with chlorambucil for 2 h, followed by **1d** and **1e** at IC_{50} concentration for 12 h. The results showed inhibitory effects on cell proliferation according to the various compounds' treatment. In combination-treated cells, a significant increase in fluorescence intensity (TUNEL-positive) compared to control cells was observed. Moreover, **1d** and **1e** individual treatments showed a slight increase in fluorescence intensity, with no such intensity being observed after individual chlorambucil treatment. As described earlier, combination treatment produces DNA double-stranded breaks. This analysis suggests that combination treatment promotes huge DNA strand breaks and DNA fragmentations, leading to apoptotic cell death.

CONCLUSIONS

In summary, we have synthesized a simple fluorescent monoquinoxaline amine **1e** that can bind and cleave abasic sites in DNA. The affinity of the amine compound **1e** is more specific toward AP-DNA compared to native DNA. The AP site's binding by **1e** induces a structural change in DNA due to stacking between the nucleobases present at AP sites. Alternately, we have demonstrated *in vitro* the reduction of the nitroquinoxaline derivative **1d** into an amine **1e** in the presence of the cellular thiol glutathione. This reduction strategy by the cellular thiol glutathione is exploited to target high glutathione-expressing cancer cells such as colon cancer cells by **1d** and **1e**, which exert cytotoxicity and DNA damage response against HCT-116 cells. These DNA damages eventually lead to DNA double-stranded breaks as determined by various methods including the Comet assay and γH2AX phosphorylation. This strategy also has a therapeutic implication, such as with the known anticancer drug chlorambucil, which in combination with either **1d** or **1e** potentiates chlorambucil's activity, causing more DNA damage altogether in colon cancer cells. The induced double-stranded break leads to G_2/M cell-cycle arrest, resulting in apoptotic cell death at submicromolar concentrations. These results suggest that the combined treatment of the nitro as well as amino compound is more effective than single treatment in HCT-116 cells. However, **1d** is more effective in terms of cytotoxicity than the amine **1e** possibly due to the hydrophobic property of the compound. Further studies are under progress to develop a class of these aminoquinoxaline derivatives targeting AP sites in specific cancer cells.

EXPERIMENTAL SECTION

Preparation of AP Sites Containing the pBR322 (AP-pBR322) Plasmid. The pBR322 plasmid was depurinated by heating at 70 °C for 17 min in 25 mM sodium phosphate buffer (pH 4.8) as described previously.[56,57] This method produced approximately 1.8 apurinic sites per DNA.

https://doi.org/10.1021/acsomega.1c04962
ACS Omega 2022, 7, 6488−6501

Investigation of DNA Cleavage Properties of 1e. **1e** (500 μM) was incubated for 16 h with the native pBR322 plasmid (1 μg) at different pH values (6.4, 7.0, 7.4) in sodium phosphate buffer (50 mM). After incubation, a loading dye was added to stop the reaction and the samples were loaded in agarose gel (1%). The gel was run in TAE buffer (1×) at 70 V for 2 h. The gel was then stained in ethidium bromide (0.5 μg/mL) aqueous solution and visualized by a Bio-Rad ChemiDoc MP Imaging System. Data were analyzed as well as quantified using Image Lab software. Next, AP-pBR322 (0.2 μg) was incubated at 37 °C for 20 min with various concentrations of **1e** in sodium phosphate buffer (50 mM, pH 7) containing NaCl (10 mM) and DMSO (1%). The reaction was stopped using 4 μL of loading buffer. Agarose (1%) in 1× TAE was prepared, and the reactions were loaded in agarose gel and run at 70 V for 2 h. The AP-DNA plasmid cleavage activity with spermine was also evaluated. The sample preparation was as described above with **1e**. The gel was visualized by the Invitrogen iBright Imaging System. For the chlorambucil reaction, the native pBR322 plasmid (1 μg) was incubated with chlorambucil (chb, 100 μM) for 3 h in sodium phosphate buffer (50 mM, pH 7) and was subsequently treated with varying concentrations of **1e** for 16 h. After incubation, a loading dye was added to stop the reaction and the samples were loaded in agarose gel (1%). The gel was run in TAE buffer (1×) at 70 V for 2 h. The gel was then stained in ethidium bromide (0.5 μg/mL) aqueous solution and visualized by the Bio-Rad ChemiDoc MP Imaging System. Data were analyzed as well as quantified using Image Lab software.

Gel Electrophoresis with ^{32}P-Labeled Oligonucleotide. The oligonucleotides used for the AP site cleavage reaction (A) 5′ GATGATAUAAGACAT 3′ and 5′ ATGTCTTGTATCATC 3′ were purchased from IDT. Then, the single-stranded oligonucleotide (A) containing the uracil residue was labeled at the 5′-end using [γ-^{32}P]-ATP and the polynucleotide kinase according to Sambrook and Russell's book.[58] Following the reaction, the oligonucleotide was annealed with the corresponding complementary oligonucleotide, which has guanine opposite to the uracil residue in 10 mM HEPES buffer (pH 7) by heating at 95 °C for 5 min followed by slowly cooling the reaction mixture. Apurinic sites were generated by treating 50 μL of uracil-containing ^{32}P-labeled annealed double-stranded oligonucleotide with 15 units of uracil-DNA glycosylase (UDG) in UDG buffer (New England Biolabs) for 30 min at 37 °C. The oligonucleotide containing the abasic site was purified using the phenol-chloroform method followed by sodium acetate (3 M, pH 5.2) precipitation.

In a typical 20 μL reaction, the abasic site containing the oligonucleotide was treated with varying concentrations of **1e** (10, 50, 100 μM) in HEPES buffer (10 mM, pH 7) at 37 °C for 16 h. In a typical imine reduction reaction, 270 mM $NaCNBH_3$ was used. An equal amount of loading dye containing formamide (95% v/v), 20 mM EDTA, bromophenol blue, and xylene cyanol (0.025% w/v) was mixed with the reaction mixture and loaded in the 20% polyacrylamide gel containing 8 M urea. The gel was run at 200 V for 4 h in 0.5× TBE buffer. The radioactive band was then visualized using a phosphorimager.

UV−Vis Spectroscopy of 1e with Native and AP-ctDNA. Interaction of **1e** with native and abasic sites containing ctDNA (AP-ctDNA) was studied via absorption spectroscopy using a 10 mm path length cuvette in a Varian spectrophotometer at 25 °C. Increasing concentrations of native ctDNA (0−60 μM bp) were titrated against **1e** (20 μM) in sodium phosphate buffer (10 mM, pH 7.0) with NaCl (10 mM) and DMSO (1%). Similarly, increasing concentrations of AP-ctDNA (0−120 μM bp) were titrated against **1e** (20 μM) in sodium phosphate buffer (10 mM, pH 7.0) with NaCl (10 mM) and DMSO (1%).

Fluorescence Spectroscopy of 1e with Native, AP-ctDNA, and THF-Containing Oligonucleotides. Fluorescence experiments were performed on a Hitachi F-7000 fluorescence spectrophotometer. The fluorescence spectra of **1e** (20 μM) were recorded at λ_{ex} = 362 μM and λ_{em} from 400 to 700 nm with increasing concentrations of native ctDNA (0−50 μM bp). Similarly, increasing concentrations of AP-ctDNA (0−60 μM bp) were titrated against **1e** (20 μM) in sodium phosphate buffer (10 mM, pH 7.0) with NaCl (10 mM) and DMSO (1%). In a separate experiment, various concentrations (0.5−3.5 μM) of four distinct oligonucleotides where different nucleobases (C, G, A, and T) were placed opposite to the AP site were titrated against **1e** (0.5 μM). In the time-dependent fluorescence experiment, **1e** (10 μM) was incubated with AP-ctDNA (50 μM bp) and the fluorescence spectra of **1e** were recorded at different time intervals (0−60 min) in sodium phosphate buffer (10 mM, pH 7.0) with NaCl (10 mM) and DMSO (1%).

Circular Dichroism (CD) of Native and AP-ctDNA with 1e and 1d. In a typical CD experiment, the native ctDNA (20 μM bp) was titrated with varying concentrations of **1e** (0−120 μM); the ellipticity was recorded using a Jasco J815 spectropolarimeter measured at 25 °C. Similarly, AP-ctDNA (20 μM bp) was titrated with increasing concentrations of **1e** (0−120 μM). CD spectra from 200 to 450 nm were recorded in a quartz cuvette (0.5 cm) with a 100 nm/min scanning rate. The experiment was conducted in sodium phosphate buffer (10 mM, pH 7.0) with NaCl (10 mM) and DMSO (1%). The CD experiment was also performed with **1d** as described above.

HPLC. A solution containing **1d** and glutathione (1:100) in sodium phosphate buffer (50 mM, pH 7) was incubated for 16 h at 37 °C. The solution was analyzed by HPLC using a C18 reverse-phase column. The gradient method (0−100%) was employed for the eluent starting from 0 to 16 min with solvent A (water) and solvent B (acetonitrile). The flow rate was maintained at 1 mL/min to monitor the products at 254 nm. Glutathione absorbance was monitored at 215 nm on the Shimadzu SCL-10A VP instrument.

Agarose Gel Electrophoresis for AP-Plasmid DNA Cleavage Activity of the 1d Reaction with Glutathione (GSH). Reactions containing **1d**, **1d** with GSH, and **1e** were separately incubated with supercoiled plasmid DNA (1 μg, pBR322) in sodium phosphate buffer (50 mM, pH 6.4) for 16 h at 37 °C. After incubation, the reactions were quenched by a loading dye (4 μL) containing bromophenol blue and xylene cyanol. Following that, the reactions were run on agarose gel (1%) at 70 V for 2 h in TAE buffer (1×). Then, the gel was stained in ethidium bromide (0.5 μg/mL) aqueous solution and visualized by the Invitrogen iBright Imaging System.

***In Vitro* Cytotoxicity.** HCT-116, A549, and HEK 293T cells were grown on collagen-coated Petri dishes in DMEM (Dulbecco's modified Eagle's medium) containing 10% FBS (fetal bovine serum) with antibiotic-antimyotic (1%) in a humidified incubator at 37 °C and 5% CO_2. After reaching

https://doi.org/10.1021/acsomega.1c04962
ACS Omega 2022, 7, 6488−6501

confluency, cells were collected by trypsin (0.025%) and EDTA (0.52 mM), resuspended in fresh media, and plated onto flat-bottom 96-well plates at a density of 5000 cells/well. The cells were incubated for an additional 24 h to allow cell attachment at the base. All of the compounds (**1d**, **1e**, chlorambucil) for treatment were prepared by dissolving in cell-culture-grade DMSO and then diluted with media without FBS and added at varying concentrations except for chlorambucil. Similar experiments were performed for other cells. For combination treatment in HCT-116 cells, initially, chlorambucil was treated at 200 μM for 2 h; after discarding the media, subsequent treatment was done with **1d** and **1e** at varying concentrations. An additional 24 h was used to incubate the plates, and cell viability was assessed by the MTT assay. After 24 h, 20 μL of MTT (5 mg/mL) was added and incubated for 3 h and the formazan formed was dissolved in 150 μL of DMSO in each well. The absorbance of the reaction was measured at 595 nm in a Thermo Scientific multiscan FFC microplate reader.

Immunofluorescence Study. HCT-116 cells were seeded at 0.3 × 10^6 cells per well in a 6-well plate containing coverslips. After 24 h, cells were treated with **1d**, **1e**, chlorambucil, and in combination for 12 h at IC_{50} concentrations. Cells were PBS-washed, fixed with paraformaldehyde (4% in PBS) for 10 min at room temperature (RT), and again washed with PBS. Cells were then permeabilized with Triton X-100 (0.5%) at RT, blocked with FBS (10% in PBS) for 1 h at 37 °C, and incubated overnight at 4 °C with a 1:1000 mouse polyclonal γ-H_2AX (Ser-139) primary antibody. Cells were washed twice with cold PBS, and antimouse secondary antibodies labeled with Alexa 555 were added at 1:1000 and incubated at 37 °C for 1 h. After incubating and staining with Hoechst, cells were spread onto glass slides using mounting solution coverslips and were mounted onto the slides. Images were acquired with an Olympus FLUOVIEW FV-10i confocal microscope.

Alkaline Comet Assay. The alkaline Comet assay is a technique to determine single-stranded break, double-stranded break, cross-links, and alkali-labile sites. The method was performed as previously described.[59] HCT-116 cells were seeded in 6-well plates overnight, and subsequently, **1d** and **1e** were added at their respective IC_{50} concentrations for 12 h. For combination treatment, cells were treated with chlorambucil for 2 h and media were removed after incubation. In fresh media, **1d** and **1e** were added separately and the treated cells were incubated separately for 12 h. Aliquots of untreated or treated cells were suspended in 1% low-melting agarose in PBS and spread onto 1% normal agarose precoated slides. The cell suspension was covered immediately with a coverslip and kept at 4 °C.

Analysis of Cell Cycle. In 6-well culture plates, HCT-116 cells were seeded and incubated with **1d**, **1e**, **1d** with chlorambucil, and **1e** with chlorambucil at their IC_{50} concentrations. After 24 h, cells were collected and fixed in 70% ethanol at 4 °C overnight. Using PBS, the cells were washed twice and incubated with propidium iodide (10 μg/mL) staining solution and RNase A (0.1 mg/mL) in the dark for 30 min at RT. The cells were analyzed in a BDLSR-Fortessa cell analyzer.

Apoptosis Analysis Using Annexin-V. In 6-well plates, HCT-116 cells were seeded and incubated with **1d**, **1e**, **1d** with chlorambucil, and **1e** with chlorambucil at their respective IC_{50} concentrations. Apoptosis was evaluated using the apoptosis detection kit (Annexin-V FITC) according to the manufacturer's instructions. Subsequently, with cold PBS, cells were washed twice and harvested. The cells (1 × 10^6) were resuspended in binding (1×) buffer. Annexin-V FITC (5 μL) and propidium iodide (1 μL) were added and incubated for 15 min at RT in the dark. The percentages of apoptotic, live, and necrotic cells were analyzed using a BDLSR-Fortessa cell analyzer.

Tunel Assay. HCT-116 cells were seeded to a coverslip in 35 mm dishes and then incubated with IC_{50} concentrations of **1d** and **1e** for 12 h. For combination treatment, cells were treated with chlorambucil for 2 h; after removing the media, **1d** and **1e** were added in fresh media and incubated for 12 h. Following incubation, they were washed in PBS; cells were then fixed with paraformaldehyde for 20 min. They were again washed with PBS and then permeabilized using Triton X-100 (0.2%) for 5 min. Subsequently, they were washed with PBS and covered with an equilibration buffer (100 μL). Then, gently a coverslip was placed to spread the buffer evenly and equilibrated for 10 min at RT. A TdT incubation buffer of 50 μL was prepared to contain the nucleotide mix, the TdT enzyme, and the equilibration buffer. After equilibration, the excess liquid was removed. The TdT incubation buffer (50 μL) was placed and incubated with a coverslip on the top in the dark for 1 h at 37 °C. The tailing reaction was terminated using 2× SSC, incubated for 15 min at RT, and followed by a PBS wash. Then, cells were stained with PI incubation for 5 min at RT. The excess stain was removed with deionized water, and using a mounting solution, the coverslips were mounted on glass slides. The slides were analyzed using an OLYMPUS FLUOVIEW FV-10i confocal microscope.

■ ASSOCIATED CONTENT

Supporting Information

The Supporting Information is available free of charge at https://pubs.acs.org/doi/10.1021/acsomega.1c04962.

> Materials, synthesis of **1e** (Scheme S1), ^{1}H-NMR of **1e** (Figure S1), ^{13}C-NMR of **1e** (Figure S2), agarose gel electrophoresis of spermine-treated AP-pBR322 plasmid DNA and **1e**-treated pBR322 plasmid DNA (Figure S3), UV−vis spectra of **1e** with native calf thymus DNA and AP-ctDNA (Figure S4), fluorescence spectra of **1e** upon addition of DNA duplex with a different base opposite the THF residue (Figure S5), time-dependent fluorescence emission spectra of **1e** with benzaldehyde (Figure S6), HPLC chromatograms of **1d** and **1e** (Figure S7), agarose gel electrophoresis of **1d** and GSH reaction (Figure S8), CD spectra of AP-CTDNA with different concentrations of **1d** (Figure S9), quantification of the γ-H2AX fluorescence intensity per HCT-116 cell (Figure S10), TUNEL assay (Figure S11), and supporting reference (PDF)

■ AUTHOR INFORMATION

Corresponding Author

Sanjay Dutta − *Organic and Medicinal Chemistry Division, CSIR-Indian Institute of Chemical Biology, Kolkata 700032 West Bengal, India; Academy of Scientific and Innovative Research (AcSIR), Ghaziabad 201002, India;* orcid.org/0000-0003-0435-5741; Email: sanjaydutta@iicb.res.in

https://doi.org/10.1021/acsomega.1c04962
ACS Omega 2022, 7, 6488−6501

Authors

Chandra Sova Mandi − *Organic and Medicinal Chemistry Division, CSIR-Indian Institute of Chemical Biology, Kolkata 700032 West Bengal, India*

Tridib Mahata − *Organic and Medicinal Chemistry Division, CSIR-Indian Institute of Chemical Biology, Kolkata 700032 West Bengal, India*

Dipendu Patra − *Organic and Medicinal Chemistry Division, CSIR-Indian Institute of Chemical Biology, Kolkata 700032 West Bengal, India; Academy of Scientific and Innovative Research (AcSIR), Ghaziabad 201002, India*

Jeet Chakraborty − *Organic and Medicinal Chemistry Division, CSIR-Indian Institute of Chemical Biology, Kolkata 700032 West Bengal, India*

Achyut Bora − *Organic and Medicinal Chemistry Division, CSIR-Indian Institute of Chemical Biology, Kolkata 700032 West Bengal, India; Academy of Scientific and Innovative Research (AcSIR), Ghaziabad 201002, India*

Ritesh Pal − *Organic and Medicinal Chemistry Division, CSIR-Indian Institute of Chemical Biology, Kolkata 700032 West Bengal, India; Academy of Scientific and Innovative Research (AcSIR), Ghaziabad 201002, India*

Complete contact information is available at: https://pubs.acs.org/10.1021/acsomega.1c04962

Notes

The authors declare no competing financial interest.

■ ACKNOWLEDGMENTS

S.D. acknowledges CSIR (MLP-139) and DST SERB (Grant No. EMR/2017/000659) for financial support. C.S.M., J.C., and A.B. acknowledge CSIR for fellowship, and R.P. acknowledges UGC for fellowship.

■ REFERENCES

(1) Loeb, L. A. Apurinic sites as mutagenic intermediates. *Cell* **1985**, *40*, 483−484.

(2) Loeb, L. A.; Preston, B. D. Mutagenesis by apurinic/apyrimidinic sites. *Annu. Rev. Genet.* **1986**, *20*, 201−230.

(3) Talpaert-Borlé, M. Formation, detection and repair of AP sites. *Mutat. Res.* **1987**, *181*, 45−56.

(4) Srivastava, D. K.; Berg, B. J.; Prasad, R.; Molina, J. T.; Beard, W. A.; Tomkinson, A. E.; Wilson, S. H. Mammalian abasic site base excision repair. Identification of the reaction sequence and rate-determining steps. *J. Biol. Chem.* **1998**, *273*, 21203−21209.

(5) Téoule, R. Radiation-induced DNA damage and its repair. *Int. J. Radiat. Biol. Relat. Stud. Phys., Chem. Med.* **1987**, *51*, 573−589.

(6) Lawley, P. D.; Brookes, P. Further studied on the alkyation of nucleic acids and their constituent nucleotides. *Biochem. J.* **1963**, *89*, 127−138.

(7) Singer, B.; Grunberger, D. *Molecular Biology of Mutagens and Carcinogens*; Plenum Press: New York, 1983.

(8) Lindahl, T.; Nyberg, B. Rate of depurination of native deoxyribonucleic acid. *Biochemistry* **1972**, *11*, 3610−3618.

(9) Nakamura, J.; Walker, V. E.; Upton, P. B.; Chirag, S. Y.; Kow, Y. W.; Swenberg, J. A. Highly sensitive apurinic/ apyrimidinic site assay can detect spontaneous and chemically induced depurination under physiological conditions. *Cancer Res.* **1998**, *58*, 222−225.

(10) Nakamura, J.; Swenberg, J. A. Endogenous apurinic/ apyimidinic sites in genomic DNA of mammalian tissue. *Cancer Res.* **1999**, *59*, 2522−2526.

(11) Strauss, B.; Hill, T. The intermediate in the degradation of DNA alkylated with a mono functional alkylating agent. *Biochim. Biophys. Acta, Nucleic Acids Protein Synth.* **1970**, *213*, 14−25.

(12) Wilde, J. A.; Bolton, P. H.; Mazumdar, A.; Manoharan, M.; Gerlt, J. A. Characterization of the equilibrating forms of the aldehydic abasic site in duplex DNA by oxygen-17 NMR. *J. Am. Chem. Soc.* **1989**, *111*, 1894−1896.

(13) Dutta, S.; Chowdhury, G.; Gates, K. S. Interstrand cross-links generated by abasic sites in duplex DNA. *J. Am. Chem. Soc.* **2007**, *129*, 1852−1853.

(14) Boiteux, S.; Laval, J. Coding properties of poly(deoxycytidylic acid) templates containing uracil or apyrimidinic sites: in vitro modulation of mutagenesis by deoxyribonucleic acid repair enzymes. *Biochemistry* **1982**, *21*, 6746−6751.

(15) Kidane, D.; Murphy, D. L.; Sweasy, J. B. Accumulation of abasic sites induces genomic instability in normal human gastric epithelial cells during Helicobacter pylori infection. *Oncogenesis* **2014**, *3*, No. e128.

(16) Bartkova, J.; Horejsí, Z.; Koed, K.; Krämer, A.; Tort, F.; Zieger, K.; Guldberg, P.; Sehested, M.; Nesland, J. M.; Lukas, C.; Ørntoft, T.; Lukas, J.; Bartek, J. DNA damage response as a candidate anti-cancer barrier in early human tumorigenesis. *Nature* **2005**, *434*, 864−870.

(17) Wei, S.; Perera, M.L.W.; Sakhtemani, R.; Bhagwat, A. S. A novel class of chemicals that react with abasic sites in DNA and specifically kill B cell cancers. *PLoS One* **2017**, *12*, No. e0185010.

(18) Pourquier, P.; Ueng, L. M.; Kohlhagen, G.; Mazumder; Gupta, M.; Kohn, K. W.; Pommier, Y. Effects of uracil incorporation, DNA mismatches, and abasic sites on cleavage and religation activities of mammalian topoisomerase I. *J. Biol. Chem.* **1997**, *272*, 7792−7796.

(19) Wilstermann, A. M.; Osheroff, N. Base excision repair intermediates as topoisomerase II poisons. *J. Biol. Chem.* **2001**, *276*, 46290−46296.

(20) Srinivasan, A.; Gold, B. Small-compound inhibitors of DNA damage-repair pathways: an approach to overcome tumor resistance to alkylating anticancer drugs. *Future Med. Chem.* **2012**, *4*, 1093−1111.

(21) Illuzzi, J. L.; Wilson, D. M. Base excision repair: contribution to tumorigenesis and target in anticancer treatment paradigms. *Curr. Med. Chem.* **2012**, *19*, 3922−3936.

(22) Li, L. Y.; Guan, Y. D.; Chen, X. S.; Yang, J. M.; Cheng, Y. DNA Repair Pathways in Cancer Therapy and Resistance. *Front. Pharmacol.* **2021**, *11*, No. 629266.

(23) Kondo, N.; Takahashi, A.; Ono, K.; Ohnishi, T. DNA damage induced by alkylating agents and repair pathways. *J. Nucleic Acids* **2010**, *2010*, No. 543531.

(24) Curtin, N. J. Inhibiting the DNA damage response as a therapeutic manoeuvre in cancer. *Br. J. Pharmacol.* **2013**, *169*, 1745−1765.

(25) Damia, G.; D'Incalci, M. Targeting DNA repair as a promising approach in cancer therapy. *Eur. J. Cancer* **2007**, *43*, 1791−1801.

(26) Male, R.; Fosse, V. M.; Kleppe, K. Polyamine-induced hydrolysis of apurinic sites in DNA and nucleosomes. *Nucleic Acids Res.* **1982**, *10*, 6305−6318.

(27) Behmoaras, T.; Toulmé, J. J.; Hélène, C. A tryptophan-containing peptide recognizes and cleaves DNA at apurinic sites. *Nature* **1981**, *292*, 858−859.

(28) Malvy, C.; Prévost, P.; Gansser, C.; Viel, C.; Paoletti, C. Efficient breakage of DNA apurinic sites by the indole-amine related 9-amino-ellipticine. *Chem.-Biol. Interact.* **1986**, *57*, 41−53.

(29) Vasseur, J. J.; Rayner, B.; Imbach, J. L.; Verma, S.; McCloskey, J. A.; Lee, M.; Chang, D. K.; Lown, J. W. Structure of the adduct formed between 3-aminocarbazole and the apurinic site oligonucleotide model d[Tp(Ap)pT]. *J. Org. Chem.* **1987**, *52*, 4994−4998.

(30) Caron, C.; Duong, X.N.T.; Guillot, R.; Bombard, S.; Granzhan, A. Interaction of functionalized napthalenophanes with abasic sites in DNA: DNA cleavge, DNA cleavage inhibition, and formation of ligand-DNA adducts. *Chem. - Eur. J.* **2019**, *25*, 1949−1962.

(31) Liu, L.; Gerson, S. L. Therapeutic impact of methoxyamine: blocking repair of abasic sites in the base excision repair pathway. *Curr. Opin. Invest. Drugs* **2004**, *5*, 623−627.

(32) Yan, L.; Bulgar, A.; Miao, Y.; Mahajan, V.; Donze, J. R.; Gerson, S. L.; Liu, L. Combined treatment with temozolomide and

https://doi.org/10.1021/acsomega.1c04962
ACS Omega 2022, 7, 6488−6501

methoxyamine: blocking apurininc/pyrimidinic site repair coupled with targeting topoisomerase II alpha. *Clin. Cancer Res.* **2007**, *13*, 1532−1539.
(33) Malvy, C.; Safraoui, H.; Bloch, E.; Bertrand, J. R. Involvement of apurinic sites in the synergistic action of alkylating and intercalating drugs in Escherichia coli. *Anti-Cancer Drug Des.* **1988**, *2*, 361−370.
(34) Fkyerat, A.; Demeunynck, M.; Constant, J. F.; Michon, P.; Lhomme, J. A new class of artificial nucleases that recognize and cleave apurinic sites in DNA with great selectivity and efficiency. *J. Am. Chem. Soc.* **1993**, *115*, 9952−9959.
(35) Mahata, T.; Kanungo, A.; Ganguly, S.; Modugula, E. K.; Choudhury, S.; Pal, S. K.; Basu, G.; Dutta, S. The Benzyl Moiety in a Quinoxaline-Based Scaffold Acts as a DNA Intercalation Switch. *Angew. Chem., Int. Ed.* **2016**, *55*, 7733−7736.
(36) Mahata, T.; Chakraborty, J.; Kanungo, A.; Patra, D.; Basu, G.; Dutta, S. Intercalator-induced DNA superstructure formation: doxorubicin and a synthetic quinoxaline Derivative. *Biochemistry* **2018**, *57*, 5557−5563.
(37) Ahammed, K. S.; Pal, R.; Chakraborty, J.; Kanungo, A.; Purnima, P. S.; Dutta, S. DNA Structural Alteration Leading to Antibacterial Properties of 6-Nitroquinoxaline Derivatives. *J. Med. Chem.* **2019**, *62*, 7840−7856.
(38) Chakraborty, J.; Kanungo, A.; Mahata, T.; Kumar, K.; Sharma, G.; Pal, R.; Ahammed, K. S.; Patra, D.; Majhi, B.; Chakrabarti, S.; Das, S.; Dutta, S. Quinoxaline derivatives disrupt the base stacking of hepatitis C virus-internal ribosome entry site RNA: reduce translation and replication. *Chem. Commun.* **2019**, *55*, 14027−14030.
(39) Berger, S. J.; Gosky, D.; Zborowska, E.; Willson, J. K.; Berger, N. A. Sensitive enzymatic cycling assay for glutathione: measurements of glutathione content and its modulation by gluthionine sulfoximine in vivo and in vitro in human colon cancer. *Cancer Res.* **1994**, *54*, 4077−4083.
(40) Barranco, S. C.; Perry, R. R.; Durm, M. E.; Quraishi, M.; Werner, A. L.; Gregorcyk, S. G.; Kolm, P. Relationship between colorectal cancer glutathione levels and patient survival: early results. *Dis. Colon Rectum* **2000**, *43*, 1133−1140.
(41) Westerfeld, W. W.; Richert, D. A.; Higgins, E. S. The metabolic reduction of organic nitro groups. *J. Biol. Chem.* **1957**, *227*, 379−391.
(42) Faguet, G. B. Chronic lymphocytic leukemia: an updated review. *J. Clin. Oncol.* **1994**, *12*, 1974−1990.
(43) Mattes, W. B.; Hartley, J. A.; Kohn, K. W. DNA sequence selectivity of guanine-N7 alkylation by nitrogen mustards. *Nucleic Acids Res.* **1986**, *14*, 2971−2987.
(44) Brookes, P.; Lawley, P. D. The reaction of mono- and di-functional alkylating agents with nucleic acids. *Biochem. J.* **1961**, *80*, 496−503.
(45) Masta, A.; Gray, P. J.; Phillips, D. R. Nitrogen mustard inhibits transcription and translation in a cell free system. *Nucleic Acids Res.* **1995**, *23*, 3508−3515.
(46) Gates, K. S. An overview of chemical processes that damage cellular DNA: spontaneous hydrolysis, alkylation, and reactions with radicals. *Chem. Res. Toxicol.* **2009**, *22*, 1747−1760.
(47) Gates, K. S.; Nooner, T.; Dutta, S. Biologically relevant chemical reactions of N7-alkylguanine residues in DNA. *Chem. Res. Toxicol.* **2004**, *17*, 839−856.
(48) Damia, G.; D'Incalci, M. Mechanisms of resistance to alkylating agents. *Cytotechnology* **1998**, *27*, 165−173.
(49) Panasci, L.; Paiement, J. P.; Christodoulopoulos, G.; Belenkov, A.; Malapetsa, A.; Aloyz, R. Chlorambucil Drug Resistance in Chronic Lymphocytic Leukemia. *Clin. Cancer Res.* **2001**, *7*, 454−461.
(50) Zhou, C.; Sczepanski, J. T.; Greenberg, M. Mechanistic studies on histone catalyzed cleavage of apyrimidinic/apurinic sites in nucleosome core particles. *J. Am. Chem. Soc.* **2012**, *134*, 16734−16741.
(51) Kanungo, A.; Patra, D.; Mukherjee, S.; Mahata, T.; Maulik, P. R.; Dutta, S. Synthesis of a visibly emissive 9-nitro-2, 3-dihydro-1 H-pyrimido [1, 2-a] quinoxalin-5-amine scaffold with large stokes shift and live cell imaging. *RSC Adv.* **2015**, *5*, 70958−70967.
(52) Takeshita, M.; Chang, C. N.; Johnson, F.; Will, S.; Grollman, A. P. Oligodeoxynucleotides containing synthetic abasic sites. Model substrates for DNA polymerases and apurinic/apyrimidinic endonucleases. *J. Biol. Chem.* **1987**, *262*, 10171−10179.
(53) Kinner, A.; Wu, W.; Staudt, C.; Iliakis, G. Gamma-H2AX in recognition and signaling of DNA double-strand breaks in the context of chromatin. *Nucleic Acids Res.* **2008**, *36*, 5678−5694.
(54) Cowell, I. G.; Sunter, N. J.; Singh, P. B.; Austin, C. A.; Durkacz, B. W.; Tilby, M. J. γH2AX foci form preferentially in euchromatin after ionising-radiation. *PLoS One* **2007**, *2*, No. e1057.
(55) Cannan, W. J.; Pederson, D. S. Mechanisms and Consequences of Double-Strand DNA Break Formation in Chromatin. *J. Cell. Physiol.* **2016**, *231*, 3−14.
(56) Constant, J. F.; O'Connor, T. R.; Lhomme, J.; Laval, J. 9-[(10-(aden-9-yl)-4,8-diazadecyl)amino]- 6-chloro-2-methoxy-acridine incises DNA at apurinic sites. *Nucleic Acids Res.* **1988**, *16*, 2691−2703.
(57) Perigolo de Oliveira, M.; Constant, J. F.; Peuchmaur, M.; Pitta, I.; Décout, J. L. Antibiotic drugs aminoglycosides cleave DNA at abasic sites: shedding new light on their toxicity? *Chem. Res. Toxicol.* **2013**, *26*, 1710−1719.
(58) Sambrook, J.; Russell, D. *Molecular Cloning: A Laboratory Manual*; Cold Spring Harbor Laboratory Press: Cold Spring Harbor, NY, 2001.
(59) Olive, P. L.; Banáth, J. P. The comet assay: a method to measure DNA damage in individual cells. *Nat. Protoc.* **2006**, *1*, 23−29.

https://doi.org/10.1021/acsomega.1c04962
ACS Omega 2022, 7, 6488−6501